Charge-Density Wave Driven Giant Thermionic-Current Switching in $1\text{T-TaS}_2/2\text{H-TaSe}_2/2\text{H-MoS}_2$ Heterostructure

Mehak Mahajan Kausik Majumdar*

Mehak Mahajan, Dr. Kausik Majumdar Department of Electrical Communication Engineering Indian Institute of Science Bangalore 560012, India

Email Address: kausikm@iisc.ac.in

 \forall Keywords: 1T-TaS₂, charge density waves, phase transitions, current switching, negative differential resistance

1T-TaS₂ exhibits several resistivity phases due to the modulation of charge density wave (CDW). The fact that such phase transition can be driven electrically has attracted a lot of attention in the recent past towards active-metal based electronics. However, the bias-driven resistivity switching is not very large (< 5 fold), and an enhancement in the same will highly impact such phase transition devices. One aspect that is often overlooked is that such phase transition is also accompanied by a significant change in the local temperature due to the low thermal conductivity of 1T-TaS₂. In this work, we exploit such electrically driven phase transition induced temperature change to promote carriers over a thermionic barrier in a 1T-TaS₂/2H-TaSe₂/2H-MoS₂ T-Junction, achieving

induced temperature due to the low thermal conductivity of 11-13-52. In this work, we exploit such earlier derivative phase transitions and 964-fold abrupt switching in the current through the MoS2 channel. The device is highly reconfigurable and exhibits an abrupt reduction in current as well when the biasing configuration changes. The results are promising for several electronic applications, including neuromorphic chips, switching, nonlinear devices, and industrial electronics such as current and temperature sensing.

1 Introduction

The charge density wave (CDW) driven phase transition in layered materials like TaS2, TaSe2, NbSe2, and TiSe2 has attracted a lot of attention in the recent past due to their structural, thermal, magnetic, electrical and optical properties [1, 2, 3, 4, 5]. Out of all these, 1T-TaS2 exhibits polymorphic states with distinctive resistive phases, that can be achieved by thermal [6, 7], mechanical [8, 9], optical [10, 11], and electrical [12, 13] excitation. On heating, 1T-TaS2 transits from commensurate (C) to triclinic (T) phase at 223 K, T to non-commensurate (NC) phase at 283 K, NC to incommensurate (IC) phase at 353 K and IC to metallic phase at 550 K. On the other hand, 2H-TaSe2 that undergoes C to NC phase transition at 90 K and NC to metallic phase at 120 K shows a slight change in slope of resistance versus temperature curve. Unlike 1T-TaS2, the resistance switching through such phase transitions can be obtained through Joule heating by electrical driving [12, 13, 14], has led to several electronic and optoelectronic device applications [15, 16, 10, 17]. The resistance switching ratio plays an important role in determining the performance of these devices. However, the degree of the resistance switching is often weak, less than 5 [12, 13, 16], depending on the flake thickness, measurement temperature, and crystal quality. Any technique that can enhance the ratio of the resistance switching will be of great importance in such phase transition-based device applications. In th

The fact that in 1T-TaS₂, the resistance switching through such phase transitions can be obtained through MoS₂ T-junction, where we achieve a gate-controllable current switching ratio up to 964 driven by CDW phase change in 1T-TaS₂ - which is more than 190-fold enhancement in the switching ratio compared to existing reports. The principle of operation of the technique exploits the abrupt change in the junction temperature due to an abrupt change in the current resulting from Joule heating induced CDW phase transition in TaS₂. This, in turn, helps to promote carriers over a thermionic barrier, modulating the net probe current. Interestingly, the proposed device is electrically reconfigurable between a positive jump (enhancement in current) and a negative jump (reduction in current). Such reduction in current can be modeled as an effective negative differential resistance (NDR), as shown earlier [17].

2 Results and Discussion

The 3D schematic diagram of the proposed triple layered T-junction is shown in **Figure 1**a. The inset of Figure 1b shows the optical image of the device D_a fabricated by exfoliating a few layer MoS₂ flake on Si/SiO₂ substrate followed by layer-by-layer dry transfer of TaSe₂ and TaS₂ flakes respectively (see the experimental section for complete fabrication steps). The current (I) - voltage (V) characteristics of the TaS₂/TaSe₂ junction of the device D_a probed between terminals T and T_S (with terminal M kept open) at 296 K are shown in Figure 1b. The abrupt hysteretic jump in the current (~ 1.24) results from the reduction in the TaS₂ resistance owing to electrically driven NC-IC CDW phase transition. Note that TaSe₂ being highly conductive, carries ample current to drive NC-IC phase transition of TaS₂ in TaS₂/TaSe₂ junction [3]. Also, the low thermal conductivity of TaSe₂ compared to Au contact further aids in raising the local temperature of the channel [18, 19]. The current jump can be further enhanced at low temperatures by invoking phase transition through multiple metastable states of TaS₂ using the external electric field [16, 10]. Figure 1c depicts the I-V characteristics of the $TaS_2/TaSe_2$ junction of the device D_a at 150 K showing a current jump of ~ 1.77 . Note that when a material with lower conductivity (such as SnSe₂) replaces the series resistance material (that is, TaSe₂), the overall current is suppressed, which reduces the Joule heating. Hence, the phase transition in TaS₂ does not occur anymore (Supplementary Figure S1).

The current-voltage characteristics of $TaSe_2/MoS_2$ junction (probed between terminals T_S and M keeping terminal T_S open) and TaS_2/MoS_2 junction (probed between terminals T and M keeping terminal T_S open) as a function of back-gate voltage (V_g) varying from -50 V to 50 V in steps of 10 V at 296 K are outlined in Figure 1d and 1e respectively. The forward and reverse sweep directions of the voltage during measurement (indicated by the black arrows in Figure 1d-e) show negligible hysteresis, suggesting excellent interface quality in the device. The corresponding gate-dependent current-voltage characteristics of both the junctions at 150 K are depicted in supplementary Figure S2a and S2b respectively.

2.1 Reconfigurable abrupt current switching in T-junction

We now show the characteristics of 1T-TaS₂/2H-TaSe₂/2H-MoS₂ T-junction that is reconfigurable between abrupt current increment and decrement by utilizing the modulation of the MoS_2 resistance through an external gate voltage. In this device, we pass a high current through a voltage bias through the TaS₂/TaSe₂ path and use the branched out MoS₂ channel current as a probe. The equivalent circuit diagram of the four terminal device D_a is shown in **Figure 2**a wherein R₁, R₂ and R₃ correspond to the effective resistance of TaSe₂, TaS₂ and MoS₂ flakes respectively. Here, R₃ includes both the TaSe₂/MoS₂ Schottky junction resistance and the MoS₂ channel resistance, and both the components are tunable by the gate voltage. A global back gate is connected to the fourth terminal of the device. Figure 2b shows the variation of MoS_2 channel current (I_M) with V_{T_S} of the device D_a when we apply the bias at T_S terminal while keeping T and M terminals grounded. The characteristics show current decrement behaviour for both $V_{T_S} < 0 \text{ V}$ and $V_{T_S} > 0 \text{ V}$ for V_q varying from -50 V to 50 V in steps of 10 V at 296 K. When the external bias exceeds the threshold voltage for the NC-IC phase transition of TaS_2 , the TaS_2 resistance abruptly reduces resulting in the abrupt increment in the TaS₂ current, and hence a simultaneous reduction in the MoS_2 current. The peak-to-valley current ratio (PVCR) obtained for $V_{T_S} < 0 \text{ V}$ and $V_{T_S} > 0$ V at 296 K are shown in bottom panel of Figure 2g. A simplistic way to further improve the PVCR values is by increasing the switching ratio of the TaS₂ resistance, which directly regulates the abrupt change in the MoS_2 current. A base temperature lower than the C-T phase transition temperature can be utilized to achieve such enhancement. We operate the device (D_a) at a temperature below the C-T transition temperature to invoke field-driven metastable states of TaS₂ that increase the abrupt current jump by $1.42\times$ in comparison to room temperature. Figure 2c depicts $I_{\rm M}$ versus $V_{\rm Ts}$ characteristics delineating current decrement at 150 K. The corresponding PVCR values at 150 K are shown in the top panel of Figure 2g reaching a maximum value of 1.27 at $V_q = -50 \text{ V}$ for $V_{T_S} > 0 \text{ V}$ which is higher in comparison to the room temperature values.

Suppose we apply the bias at the TaS₂ terminal while keeping terminals T_S and M grounded as depicted

in the equivalent circuit in Figure 2d. In that case, the MoS₂ current exhibits an abrupt increment instead of a decrement at the phase transition. When we apply a high electric field across the TaS₂/TaSe₂ junction, the TaS₂ phase transition occurs, which reduces the resistance of the TaS₂ branch resulting in the abrupt increment in the TaS₂ current as well as the MoS₂ current. Here, the total current flow through R₂ instead of R₁ (in the case of TaSe₂ biasing) as shown by the arrows in Figure 2d. Figure 2e and 2f shows the gate voltage (V_q) dependent current increment characteristics for both $V_T < 0 V$ and $V_T > 0$ V at 296 K and 150 K, respectively. The corresponding current increment factor as the function of V_q for both 296 K and 150 K is shown in Figure 2h. Current increment factor reaches a maximum value of ~ 4 at 150 K for $V_T > 0$ V which is $\sim 2.75 \times$ higher than the room temperature value. The low-temperature current increment factor of 4 cannot solely result from phase transition induced resistance switching of TaS₂ as it is limited to a factor of ~ 1.77 as shown in Figure 1c. In addition to 1T-TaS₂, 2H-TaSe₂ also exhibits CDW phase transitions at 90 K and 120 K. However, it does not cause any abrupt discontinuity in the TaSe₂ resistance apart from a slight slope change in resistance versus temperature curve [20, 21, 3]. The overall change in resistance of the TaSe₂ branch from the estimated temperature values (discussed later) is small and rules out the contribution of TaSe₂ resistance change to the current jump. Also, the heat equation solution of the channel and the in-situ Raman measurement exclude the possibility of structural phase transition of MoS₂ from the semiconducting (2H) to metallic (1T) phase. The abrupt current increment due to the TaS₂ phase transition increases the local temperature along the device channel. The one-dimensional heat equation solution (using FEM) for the TaS₂/TaSe₂ channel estimates that the local temperature increment due to Joule heating is sufficient to invoke TaS₂ phase transitions (see Supplementary Figure S3), depending upon the base temperature as well as the external bias. However, it is not enough to induce structural 2H to 1T phase transition in MoS₂ [22]. This argument is further supported by bias-dependent Raman measurement (see Supplementary Figure S4), wherein j-peaks have not been observed, which could otherwise confirm the presence of the 1Tphase of MoS_2 .

Such a large current increment can be explained by the enhanced thermionic carrier injection across the TaSe₂/MoS₂ barrier with a sudden increase in the junction temperature resulting from the Joule heating induced phase transitions of TaS₂, as detailed next. The mechanism is schematically illustrated in Figure 3a-b. The abrupt jump in temperature due to the CDW phase transition in TaS₂ causes a corresponding increment in temperature at the TaSe₂/MoS₂ junction due to efficient heat conduction through the TaS₂/TaSe₂ interface. That, in turn, enhances the kinetic energy of the carriers, helping them overcome the TaSe₂/MoS₂ Schottky barrier.

2.2 Giant current increment driven by thermionic switching

To explore the thermionic effect due to local temperature switching, we fabricate another triple layered T-junction (D_b) comprising a narrow MoS₂ channel with a reduced junction overlap area (see the optical image in the inset of Figure 4a). Here we choose a small junction overlap area between MoS₂ and the TaS₂/TaSe₂ to further increase the temperature by forcing the hot electrons to pass through a smaller region. Apart from weaker heat dissipation efficiency, the smaller junction area helps in two other ways. First, when the junction area is small, the fractional contribution of the junction resistance to the total device resistance increases. That helps to achieve a larger switching ratio since the hot carriers, due to the phase transition-induced temperature change, primarily modulate the junction resistance. Second, a smaller overlap area helps to remove any trapped residue and air from the interface during annealing, which in turn helps to achieve closer proximity between MoS₂ and TaSe₂/TaS₂ heater, helping the MoS₂ layer to achieve a higher temperature effect at the junction during the switching. I_M versus V_T of device D_b for selective V_g values varying from 20 V to 50 V (step size: 10 V) at 300 K for $V_T < 0$ V is depicted in Figure 4a. Similarly, Figure 4b shows the I_M versus V_T for $V_T > 0$ at V_g equal to 0 V, 30 V and 50 V. The corresponding current increment factors during the phase transition are plotted in Figure 4c showing a maximum value of ~ 3 at $V_g = -10$ V for $V_T > 0$ V at 300 K which is $2 \times$ higher in comparison to the current increment factor of device D_a.

At low temperature, we could further enhance the current jump as depicted in I_M versus V_T character-

istics of device D_b at 77 K (see Figure 4d and 4e for $V_T < 0$ V and $V_T > 0$ V, respectively) for different V_g values. The corresponding current increment factors are plotted in Figure 4f for both $V_T < 0$ V and $V_T > 0$ V. We could enhance the MoS_2 current by a factor of ~ 964 at $V_g = 10$ V for $V_T > 0$ V as represented in Figure 4f. As discussed earlier, such a huge jump can not solely arise from electrically driven TaS_2 phase transition. And, we must invoke the corresponding sudden rise in the junction temperature due to the abrupt enhancement in current through $TaS_2/TaSe_2$ during the CDW phase transition of TaS_2 . Figure 4g depicts the variation of the current increment factor as a function of V_g at a base temperature of 77 K, 120 K, and 160 K for $V_T > 0$ V. Such a strong temperature dependence in the current increment factor suggests possible usage of the technique in sensing temperature.

In Figure 4f for $V_T > 0$, the current jump ratio at the phase transition exhibits a strong non-monotonic behavior with V_g . Also, the ratio shows an opposite trend for $V_T < 0$, particularly when $V_g < 0$. The origin of such behavior is explained in Figure 5. In the case of $V_T > 0$ V, that is, when MoS_2 injects electrons into TaSe₂, there are three different regions of device operation (viz. A, B, and C as shown in Figure 4c and 4f) as schematically explained in Figure 5a. Note that, due to the high electrical conductivity of TaSe₂ in comparison to TaS₂ (in particular, at a low temperature), the floating voltage at the triple junction is small; hence the drop across the MoS_2 channel is also small (estimated to be < 26mV). Due to such a small effective drain voltage, the current through the MoS₂ channel strongly depends on the drain barrier as well in the different regimes of operation. In the current situation, where TaSe₂ acts as the drain contact for $V_T > 0$ configuration, the drain barrier plays an even more important role. We recently found that due to van der Waals nature of the contact interface, TaSe₂ exhibits strong Fermi level depinning [23] with layered semiconductors. Accordingly, due to the relatively large work function of TaSe₂, the conduction band offset between MoS₂ and TaSe₂ is large. On the other hand, due to Fermi level pinning, Ni/MoS₂ junction has a relatively small Schottky barrier height [24]. That leads to a larger drain barrier compared to the source barrier at the small effective drain bias as schematically shown in Figure 5a, and hence the TaSe₂/MoS₂ interface controls the drain current.

In region A, that is, for $V_q \ll 0$ V, electrons do not see any barrier at the drain side and can quickly transfer into TaSe₂ (see top panel of Figure 5a). Thus, the current does not change much with the abrupt increase in temperature during the CDW phase transition. In region B, the electrons from the MoS₂ region require to overcome the drain barrier to be transferred to TaSe₂ (see middle panel of Figure 5a), and thus the current is a strong function of the local temperature at the drain barrier. The current induced Joule heating can increase the local temperature to $\sim 230~\mathrm{K}$ for a base temperature of 77 K (see Supplementary Figure S3 for simulated results). The current jump ratio simulated for various barrier heights (ϕ_b varying from 30 to 80 meV) by solving modified Richardson's equation [24] at temperatures of 120 K, 150 K, 180 K, 210 K and 240 K with respect to 77 K is shown in Supplementary Figure S5. The simulation results clearly show that the current ratio before and after the phase transition can go as high as 10^4 depending upon ϕ_b . That justifies the high current increment factor at $V_g = 10$ V. Finally, in region C for $V_q \gg 10$ V, the band bending increases, and the electrons can tunnel through the Schottky drain barrier, as shown in the bottom panel of Figure 5a. Thus, the local temperature does not affect the current, reducing the current ratio before and after the phase transition. Beyond region C, at an even higher positive V_q , we observe an increment in the current increment factor, the origin of which is yet not very clear and could result from a V_q dependent change in the relative resistance between the source and the drain barriers.

On the other hand, for $V_T < 0$ V, TaSe₂ acts as a source contact, and the electrons are injected from TaSe₂ to the MoS₂ channel. At high negative V_g , i.e., region D, the carrier injection is determined by thermionic transport over the Schottky barrier height at TaSe₂/MoS₂ interface, as shown in the top panel of Figure 5b, and hence contributes to higher current jump. However, for $V_g > 0$ V (region E), the current increment ratio decreases monotonically as the carrier injection is dominated by the tunneling phenomenon schematically shown in the bottom panel of Figure 5b.

In similarity to device D_a , the I_M versus V_{T_S} characteristics of device D_b exhibits current decrement for V_{T_S} biasing at both 300 K and 77 K (see Supplementary Figure S6). The corresponding I_M versus V_T (depicting current increment) and I_M versus V_{T_S} (depicting current decrement) characteristics for device

D_b at 120 K and 160 K are outlined in Supplementary Figure S7 and S8 respectively. The current increment characteristics have been repeatedly observed in several devices, some of which are outlined in Supplementary Figure S9 and S10.

3 Conclusion

The technique proposed in this work demonstrates a unique way of significantly amplifying the resistance switching ratio typically obtained from a TaS₂ CDW phase transition. That is achieved by exploiting enhanced carrier injection through a Schottky barrier height by the abrupt increment in the local temperature during the phase transition. Accordingly, the technique can be applied to enhance the device performance in several applications where TaS₂ phase transition is used, for example, in detecting infrared photons and neuromorphic applications. In addition, the gate tunable sharp jump in current can be useful for sensing applications, such as temperature and current. On the other hand, the enhancement in the MoS₂ channel current during the CDW phase transition of TaS₂ provides an excellent probe to monitor the local temperature of TaS₂.

4 Experimental Section

Triple Layered T-Junction Device Fabrication and characterization.: 1T-TaS₂/2H-TaSe₂/2H-MoS₂ T-junction is fabricated in the following manner. First, the thin flakes of MoS₂ are mechanically exfoliated on a heavily doped Si substrate coated with 285 nm thick SiO₂ using polydimethylsiloxane (PDMS), followed by dry transfer of TaSe₂ and TaS₂ flakes respectively. A rotational stage controls the alignment during each layer transfer to form the T-junction. The complete exfoliation and dry transfer processes are done at room temperature. The substrate is then spin-coated with a high contrast positive resist — polymethyl methacrylate (PMMA) 950 C3 and softly baked for 2 minutes at 180 °C. Patterns are formed through electron beam lithography with an electron beam dose of 200 μ C cm⁻², an electron beam current of 300 pA, and an acceleration voltage of 20 KV. The pattern development is carried out in 1 : 3 MIBK/IPA developer solution followed by IPA wash and blow drying in N₂. Metal contacts are formed by blanket deposition of 10 nm Ni / 50 nm Au using a DC magnetron sputter coating system in the presence of Ar plasma at 6.5×10^{-3} Torr. Excess metal lift-off is carried out by immersing the substrate in acetone for 15-30 minutes, followed by IPA wash for 30 seconds and blow drying in N₂. Buffered HF solution is used to etch the back oxide from the substrate, and highly conducting silver paste is used for the back gate contact.

The electrical measurements are carried out in a probe station with a base vacuum level of about 1.6×10^{-3} Torr at room temperature and 6.45×10^{-6} Torr at the low temperature with the supply of liquid N_2 .

Supporting Information

Supporting Information is available from the Wiley Online Library or from the author.

Acknowledgements

This work was supported in part by a Core Research Grant from the Science and Engineering Research Board (SERB) under Department of Science and Technology (DST), a grant from Indian Space Research Organization (ISRO), a grant from MHRD under STARS, and a grant from MHRD, MeitY and DST Nano Mission through NNetRA.

References

[1] M. S. El-Bana, D. Wolverson, S. Russo, G. Balakrishnan, D. M. Paul, S. J. Bending, Superconductor Science and Technology 2013, 26, 12 125020.

[2] B. Yan, B. Zhang, H. Nie, G. Li, X. Sun, Y. Wang, J. Liu, B. Shi, S. Liu, J. He, Nanoscale 2018, 10 20171.

- [3] M. Mahajan, S. Kallatt, M. Dandu, N. Sharma, S. Gupta, K. Majumdar, *Communications Physics* **2019**, 2, 188.
- [4] E. Zhang, X. Xu, Y.-C. Zou, L. Ai, X. Dong, C. Huang, P. Leng, S. Liu, Y. Zhang, Z. Jia, X. Peng, M. Zhao, Y. Yang, Z. Li, H. Guo, S. J. Haigh, N. Nagaosa, J. Shen, F. Xiu, *Nature Communications* 2020, 11, 1 5634.
- [5] W. Li, G. V. Naik, Applied Physics Letters **2021**, 118, 25 253104.
- [6] R. Manzke, T. Buslaps, B. Pfalzgraf, M. Skibowski, O. Anderson, Europhysics Letters (EPL) 1989, 8, 2 195.
- [7] A. H. Thompson, R. Gamble, J. Revelli, Solid State Communications 1971, 9 981.
- [8] K. Bu, W. Zhang, Y. Fei, Z. Wu, Y. Zheng, J. Gao, X. Luo, Y.-P. Sun, Y. Yin, Communications Physics 2019, 2, 1 146.
- [9] S. S, H. K. Kundu, P. Vishnubhotla, A. Bid, Phys. Rev. Materials 2021, 5 124003.
- [10] C. Zhu, Y. Chen, F. Liu, S. Zheng, X. Li, A. Chaturvedi, J. Zhou, Q. Fu, Y. He, Q. Zeng, H. J. Fan, H. Zhang, W.-J. Liu, T. Yu, Z. Liu, ACS Nano 2018, 12, 11 11203.
- [11] W. Li, G. V. Naik, Nano Letters **2020**, 20, 11 7868, pMID: 32816498.
- [12] M. J. Hollander, Y. Liu, W.-J. Lu, L.-J. Li, Y.-P. Sun, J. A. Robinson, S. Datta, Nano Letters 2015, 15, 3 1861.
- [13] M. Yoshida, T. Gokuden, R. Suzuki, M. Nakano, Y. Iwasa, Phys. Rev. B 2017, 95 121405.
- [14] M. Mahajan, K. Murali, N. Kawatra, K. Majumdar, Phys. Rev. Applied 2019, 11 024031.
- [15] M. Yoshida, R. Suzuki, Y. Zhang, M. Nakano, Y. Iwasa, Sci Adv 2015, 1, 9 e1500606.
- [16] G. Liu, B. Debnath, T. R. Pope, T. T. Salguero, R. K. Lake, A. A. Balandin, Nature Nanotechnology 2016, 11, 10 845.
- [17] M. Mahajan, K. Majumdar, ACS Nano 2020, 14, 6 6803, pMID: 32406676.
- [18] M. D. Núñez Regueiro, J. M. Lopez-Castillo, C. Ayache, Phys. Rev. Lett. 1985, 55 1931.
- [19] B. Huettner, Femtosecond Laser Pulse Interactions with Metals, 315–337, ISBN 978-1-4020-9339-5, 2009.
- [20] H. N. S. Lee, M. Garcia, H. L. McKinzie, A. Wold, Journal of Solid State Chemistry 1970, 1 190.
- [21] M. Naito, S. Tanaka, Journal of the Physical Society of Japan 1982, 51, 1 219.
- [22] D. Y. Hwang, K. Choi, D. Suh, Nanoscale **2018**, 10.
- [23] K. Murali, M. Dandu, K. Watanabe, T. Taniguchi, K. Majumdar, 2021.
- [24] D. Somvanshi, S. Kallatt, C. Venkatesh, S. Nair, G. Gupta, J. K. Anthony, D. Karmakar, K. Ma-jumdar, Phys. Rev. B 2017, 96 205423.

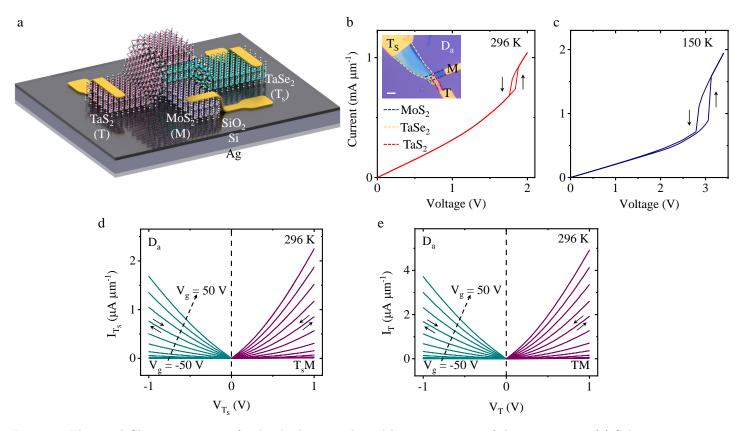


Figure 1: Electrical Characterization of individual materials and heterojunctions of the T-junction. (a) Schematic representation of triple layered T-junction. The Ag contact is used as a global back gate.(b) Current-voltage characteristics of two-probe $TaS_2/TaSe_2$ junction (probed between terminals T_S and T of D_a) indicating the NC-IC phase transition of TaS_2 at 296 K. Inset: The optical image delineating each layer of the fabricated triple layered T-junction (D_a) (Scale bar: 5 μm). (c) Current-voltage characteristics of $TaS_2/TaSe_2$ junction at 150 K. Forward and reverse sweeps are indicated by black arrows. (d) I-V characteristics of $TaSe_2/MoSe_2$ junction, probed between terminals T_S and M keeping terminal T open, for V_g varying from -50 V to 50 V in steps of 10 V at 296 K. (e) I-V characteristics of $TaSe_2/MoSe_2$ junction, probed between terminals T and M keeping terminal T_S open, as a function of V_g varying from -50 V to 50 V in steps of 10 V at 296 K.

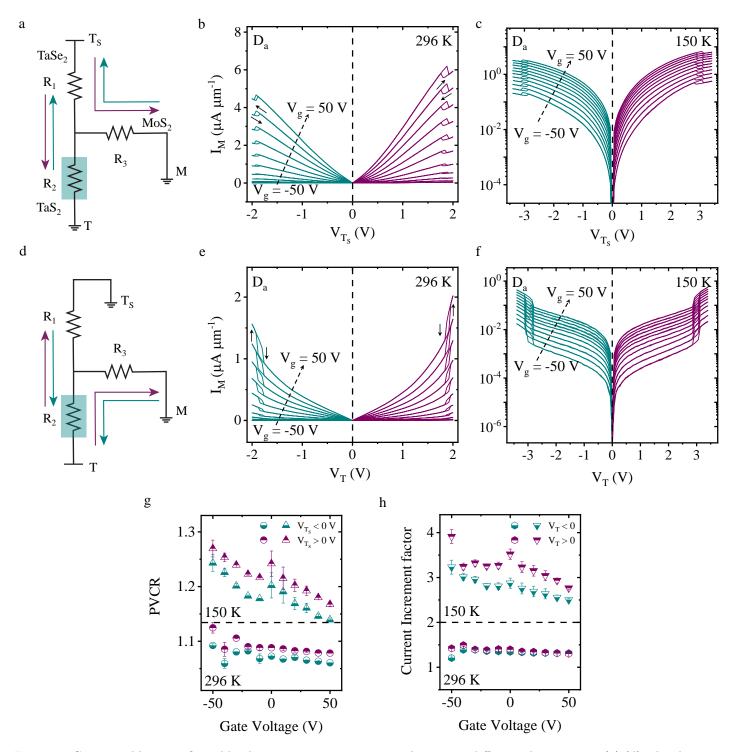
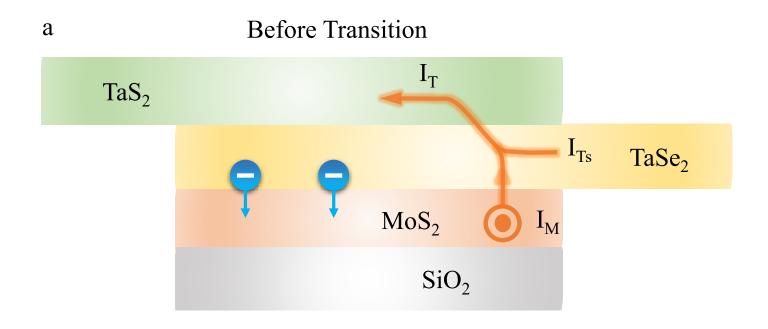


Figure 2: Gate-tunable, reconfigurable abrupt current increment and negative differential resistance. (a),(d) The three branches of the device D_a depicted by three effective resistances R_1 , R_2 and R_3 , corresponding to $TaSe_2$, TaS_2 and MoS_2 , respectively, for $TaSe_2$ (T) biasing [in (a)] and TaS_2 (T_S) biasing [in (d)]. R_3 includes the MoS_2 branch resistance and the $TaSe_2/MoS_2$ Schottky junction resistance. The cyan box (in the $TaSe_2$ branch) indicates the branch where CDW phase transition occurs. The arrows indicate the direction of the current flow in different biasing configurations. (b),(c) Current through the MoS_2 branch (I_M) versus V_{T_S} as a function of V_g varying from -50 V to 50 V in steps of 10 V at 296 K and 150 K depicting current decrement for both $V_{T_S} > 0$ and $V_{T_S} < 0$. Forward and reverse sweeps are indicated by black arrows. (e),(f) I_M versus V_T as a function of V_g varying from -50 V to 50 V in steps of 10 V at 296 K and 150 K depicting abrupt current increment for both $V_T > 0$ and $V_T < 0$. Forward and reverse sweeps are indicated by black arrows. (g) Peak-to-valley current ratio (PVCR) as the function of V_g at 296 K and 150 K in bottom and top panel respectively. (h) Current increment factor as a function of V_g at 296 K and 150 K in bottom and top panel respectively.



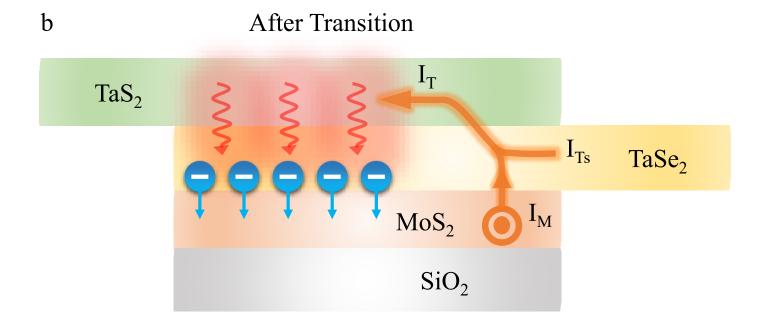


Figure 3: Schematic illustration of the mechanism. Schematic representation of the situation (a) before and (b) after the CDW phase transition in TaS_2 . The orange arrow and the out-of-plane direction symbol indicate the direction of the current flow though the junction and in the MoS_2 channel, respectively. The heat flow from TaS_2 to the $TaSe_2/MoS_2$ junction in (b) is indicated by the red curved arrows. The abrupt enhancement in temperature promotes a larger number of electrons through the $TaSe_2/MoS_2$ Schottky barrier, in turn causing an abrupt change in the MoS_2 channel current.

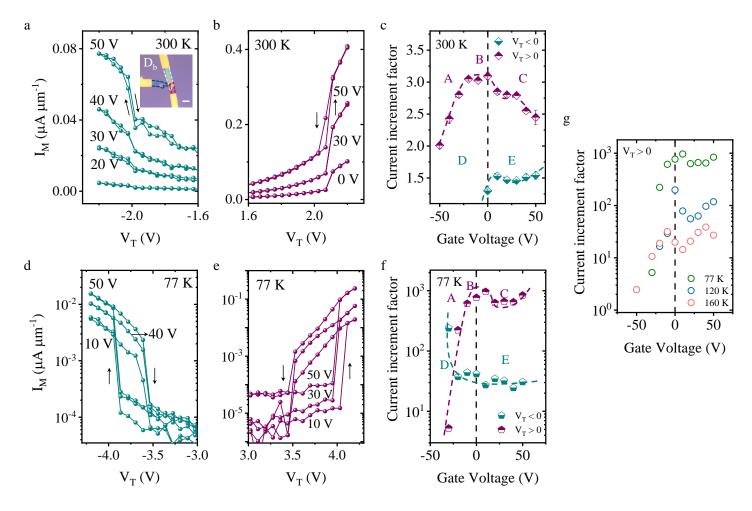
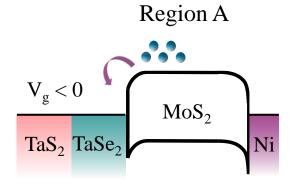
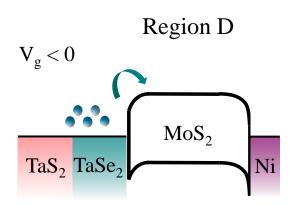


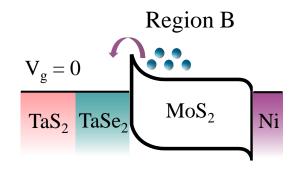
Figure 4: Giant current increment in triple layered junction. (a), (b) I_M versus V_T for selected V_g at 300 K for $V_T < 0$ [in (a)] and $V_T > 0$ [in (b)] depicting abrupt current increment. Forward and reverse sweeps are indicated by black arrows. The inset of (a) shows the optical image of the fabricated triple layered T-junction (D_b) (Scale bar: 5 μ m). (d),(e) I_M versus V_T for selected V_g at 77 K for $V_T < 0$ [in (d)] and $V_T > 0$ [in (e)] depicting abrupt current increment. (c),(f) Current increment factor as the function of V_g at 300 K [in (c)] and 77 K [in (f)] extracted from (a),(b) and (d),(e) respectively. (g) Current increment factor as a function of V_g at 77, 120 and 160 K.

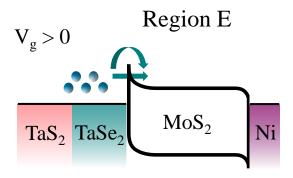
a MoS_2 Injection $(V_T > 0)$

b TaS_2 Injection $(V_T < 0)$









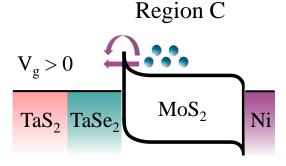
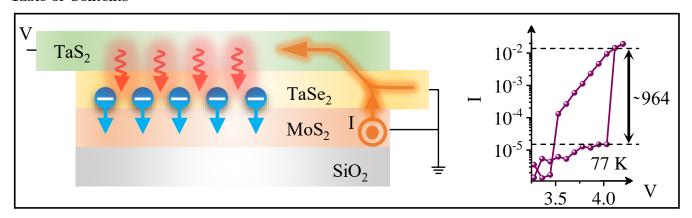


Figure 5: Thermionic switching behavior. (a) Band alignment schematics for $V_T>0$, that is, when MoS_2 injects electron into $TaSe_2$ through the drain barrier at $V_g<0$ (in top panel), $V_g=0$ (in middle panel), and $V_g>0$ (in bottom panel) corresponding to region A, B, and C in figure 4. (b) Band diagram for $TaSe_2$ injection into MoS_2 through the source barrier $(V_T<0)$ for $V_g<0$ (in top panel), and $V_g>0$ (in bottom panel) illustrating region D and E from Figure 4c and f.

Table of Contents



The electrically driven phase transition of $1\,T\text{-}\mathrm{TaS}_2$ and the low thermal conductivity of $2H\text{-}\mathrm{TaSe}_2$ are exploited in a local heater structure to achieve a 964-fold abrupt current enhancement through the MoS_2 channel in a $1T\text{-}\mathrm{TaS}_2/2H\text{-}\mathrm{TaSe}_2/2H$ - MoS_2 T-junction. The device is highly reconfigurable and exhibits a sharp reduction in current when the biasing configuration changes. In addition, the gate tunability of the current jump makes it useful for various sensing applications, including current and temperature sensors.